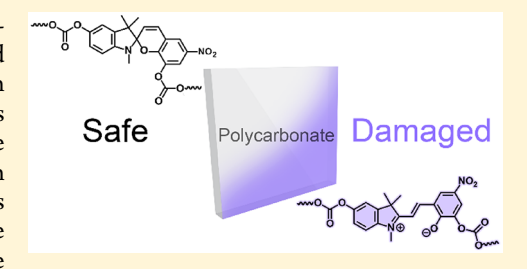


# **Enabling Room-Temperature Mechanochromic Activation in a** Glassy Polymer: Synthesis and Characterization of Spiropyran **Polycarbonate**

Yuval Vidavsky, †, || Steven J. Yang, †, || Brooks A. Abel, † Iris Agami, Charles E. Diesendruck, Geoffrey W. Coates, and Meredith N. Silberstein\*, †

Supporting Information

ABSTRACT: Mechanochromic functionality realized through force-responsive molecules (i.e., mechanophores) has great potential for spatially localized damage warning in polymers. However, in structural plastics, for which damage warning is most critical, this approach has had minimal success because brittle failure typically precedes detectable color change. Herein, we report on the room-temperature mechanochromic activation of spiropyran in high  $T_{\sigma}$  bisphenol A polycarbonate. The mechanochromic functionality was introduced by polymerization of dihydroxyspiropyran as a comonomer while retaining the excellent thermomechanical properties of the polycarbonate. The



mechanochromic behavior is thoroughly evaluated in response to changes in stress, deformation, and time, providing new insights regarding how loading history controls stress accumulation in polymer chains. In addition, a new method to incorporate mechanochromic functionality in structures without dispersing costly mechanophores in the bulk is demonstrated by using a mechanochromic laminate. The room-temperature mechanochromic activation in a structural polymer combined with the new and efficient preparation and processing methods bring us closer to the application of mechanochromic smart materials.

#### INTRODUCTION

In the field of stimuli-responsive materials, there is a growing interest in compounds that can generate productive chemical transformations in response to mechanical load, that is, mechanophores. 1-6 Particularly, mechanophores that boast the ability to display mechanically driven color or emission change have been suggested as sensors for stress, strain, and damage detection in polymeric materials.<sup>7–9</sup> Furthermore, these mechanophores can be used as molecular probes to illuminate the microscopic processes that govern the transmission of mechanical energy from external stress to deformation and force along polymer chains.<sup>4,9-14</sup> One of the most ubiquitous and well-studied mechanophores is spiropyran (SP). 15,16 SP demonstrates a distinct color and fluorescence change under mechanical stimulus due to breaking of the weak C<sub>spiro</sub>-O bond and isomerization to merocyanine (MC). 16 SP can be covalently incorporated into polymers via different anchor points that result in different activation responses. 12,17 Moreover, SP can be incorporated into polymers using different attachment chemistries 15,18-20 as well as by various attachment mechanisms (initiator, <sup>20,21</sup> cross-linker, <sup>16,22–24</sup> or monomer<sup>25</sup>).

However, there are major challenges that inhibit application of SP as a sensor in polymeric materials. While the activation of SP at room temperature in rubbery materials is quite common, 14,21,24,26 the ability to activate SP at room temperature in glassy polymers has remained mostly elusive. 8,27,28 SP activation in glassy polymers has only been achieved by specially designed force application methods including torsional shearing<sup>29</sup> and high amplitude acoustic shockwaves.<sup>2</sup> This limitation happens because brittle failure often occurs before mechanochromic activation. 15 While tensile SP activation in glassy polymers can be achieved at elevated temperature  $^{28,30}$  or by the addition of plasticizers,  $^{26}$  these methods deteriorate the mechanical properties of the material and are not representative of standard working conditions. For mechanophores to serve as damage warning sensors in highperformance structural plastics, the mechanochromic activation needs to be tailored to the application. Hence, a basic understanding of how force is transmitted and accumulated is fundamental to the development of precise mechanochromic systems.<sup>31,32</sup> Given that there is a complex relationship between mechanochromic response and stress, deformation, and time, understanding the transformation in varying mechanical conditions is essential.<sup>30</sup>

Currently, the synthesis of mechanophores and the incorporation into polymeric materials is laborious.<sup>4</sup> For example, the overall yield for the synthesis of spiropyran with bis(methacrylate) side groups is ~4% mainly due to the

Received: April 18, 2019 Published: June 6, 2019



<sup>&</sup>lt;sup>†</sup>Sibley School of Mechanical and Aerospace Engineering, and <sup>‡</sup>Department of Chemistry and Chemical Biology, Baker Laboratory, Cornell University, Ithaca, New York 14853-1301, United States

Schulich Faculty of Chemistry, Technion — Israel Institute of Technology, Haifa 3200003, Israel

$$O_2N \longrightarrow O_1 \longrightarrow O_2N \longrightarrow O_2N \longrightarrow O_2N \longrightarrow O_2N \longrightarrow O_2N \longrightarrow O_1-x$$
 
$$SP(OH)_2 \longrightarrow BPA$$
 
$$SP-BPA-PC \times = 0.001$$

Figure 1. Synthesis of spiropyran-bisphenol A polycarbonate (SP-BPA-PC) by the copolycondensation of bisphenol A (BPA), dihydroxyspiropyran (SP(OH)<sub>2</sub>), and triphosgene in dichloromethane with triethylamine (Et<sub>3</sub>N).

inefficient final substitution step of dihydroxyspiropyran. 16,33 In polycondensations, the dihydroxyspiropyran can be directly used, significantly improving the yield of the chemical process.<sup>34</sup> Moreover, the mechanophores are typically uniformly dispersed throughout the polymer. However, mechanophores could be used more efficiently by direct deposition in specific domains by 3D printing<sup>35</sup> or by the development of mechanochromic coatings.<sup>36</sup>

We have addressed the challenges described above by embedding SP functionality into bisphenol A polycarbonate (BPA-PC) backbone. BPA-PC is an engineering thermoplastic that boasts a high glass transition temperature  $(T_{\sigma})$ , strength, toughness, impact resistance, and optical transparency.<sup>37</sup> It can be readily synthesized, processed, and molded. Because of these properties, polycarbonate is being used in safety-critical applications such as protective gear, 38° aviation, 39 and bullet resistant glass. 40 The ability to detect damage in advance before catastrophic failure is highly desirable for these applications.

Herein, we present the synthesis of high molecular weight BPA-PC with SP functionality embedded in its backbone. The low yield SP functionalization step is avoided by using dihydroxyspiropyran as a bisphenol comonomer. The copolymer retains the high performance mechanical and thermal properties of polycarbonate while presenting the desired mechanochromic activation at room temperature. We investigate the influence of stress, deformation sequence, and time on the activation of SP. We also demonstrate the use of a mechanochromic laminate as an economical alternative to the uniform dispersion of mechanophores throughout the bulk.

# ■ RESULTS AND DISCUSSION

Spiropyran-Bisphenol A Polycarbonate (SP-BPA-PC) Synthesis. Spiropyran-bisphenol A polycarbonate (SP-BPA-PC) was synthesized by a modification to the industrial polycarbonate production process<sup>37</sup> that involves the reaction of phosgene with bisphenol A in CH2Cl2 under basic conditions (Figure 1). Triphosgene was used instead of the direct addition of the highly toxic phosgene gas. 41 Dihydroxyspiropyran (SP(OH)<sub>2</sub>) was synthesized according to the literature procedure<sup>34</sup> (see Supporting Information) and used directly as a bisphenol comonomer. Because triphosgene can react as three phosgene molecules 42 (Figure S3), triphosgene use will be noted according to its phosgene equivalents.

While the SP-BPA-PC synthesized by the method described above reached the desired molecular weight, it did not show the expected SP (colorless) to MC (purple) photochromic isomerization in solution on exposure to 365 nm UV light, typically observed for SP-containing polymers (Figure 2). Because of the SP-MC equilibrium in solution, under excess phosgene conditions ([phosgene] > [phenol]), either chlor-

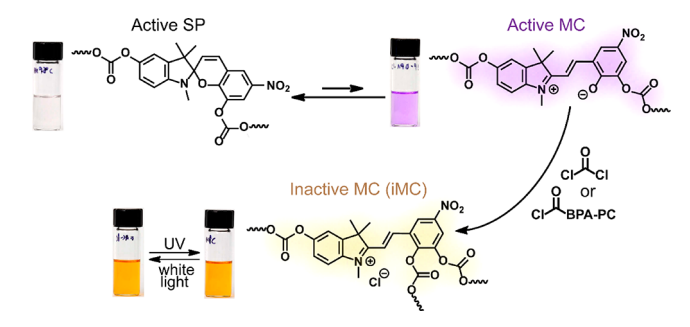


Figure 2. SP-MC equilibrium generates a MC phenoxide functionality that in turn reacts with chloroformate end-groups or phosgene to produce permanently inactive merocyanine (iMC) species. The top vials show the typical color change between active SP (colorless) and MC (purple). The iMC (yellow) does not show a visible color change under UV or white light exposure.

oformate polymer chain-ends or phosgene react with the transient MC phenoxide. The reaction of the phenoxide fixates the MC in an inactive (iMC) configuration and prevents the reversible force and light-induced isomerization (Figure 2). White light irradiation during the polymerization reaction to shift the SP-MC equilibrium to the ring-closed SP configuration<sup>43</sup> showed only limited success in preventing the unwanted side reaction (Figure S4).

We next sought to minimize formation of the iMC species by synthesizing SP-BPA-PC under phosgene-starved conditions. The MC-derived phenoxide is located para to the NO<sub>2</sub> group and is therefore less nucleophilic as compared to the BPA and SP(OH)2-derived phenoxides (Figure 3a) as indicated from the calculated  $pK_a$  values of the conjugate phenols<sup>44</sup> (Figure S5). As a result of this reactivity difference, <sup>45</sup> iMC formation was effectively suppressed by performing the reaction under phosgene-starved conditions (Figure 3b). However, only low molecular weight SP-BPA-PC was obtained when using nonstoichiometric reaction conditions ([phosgene]/[BPA] < 1). The lower molecular weight SP-BPA-PC is a brittle material in contrast to the high toughness typically associated with commercial polycarbonate. To achieve high molecular weight PC without iMC formation, small amounts of triphosgene ([phosgene] = 1/2[phenol] end-groups) were added stepwise to the low molecular weight SP-BPA-PC (Figure 3b). The stepwise addition of triphosgene was performed while monitoring the molecular weight by gel permeation chromatography (GPC). Figure 3c shows the reduction in retention time after each addition of triphosgene, while Figure 3d shows the corresponding increase in numberaverage molecular weight  $(M_n)$ . The synthesized PC was confirmed by <sup>1</sup>H and <sup>13</sup>C NMR (Figures S6 and S7) and presented the typical thermal and mechanical properties (Figures S8 and S9) for BPA-PC. Satisfactorily, a solution of

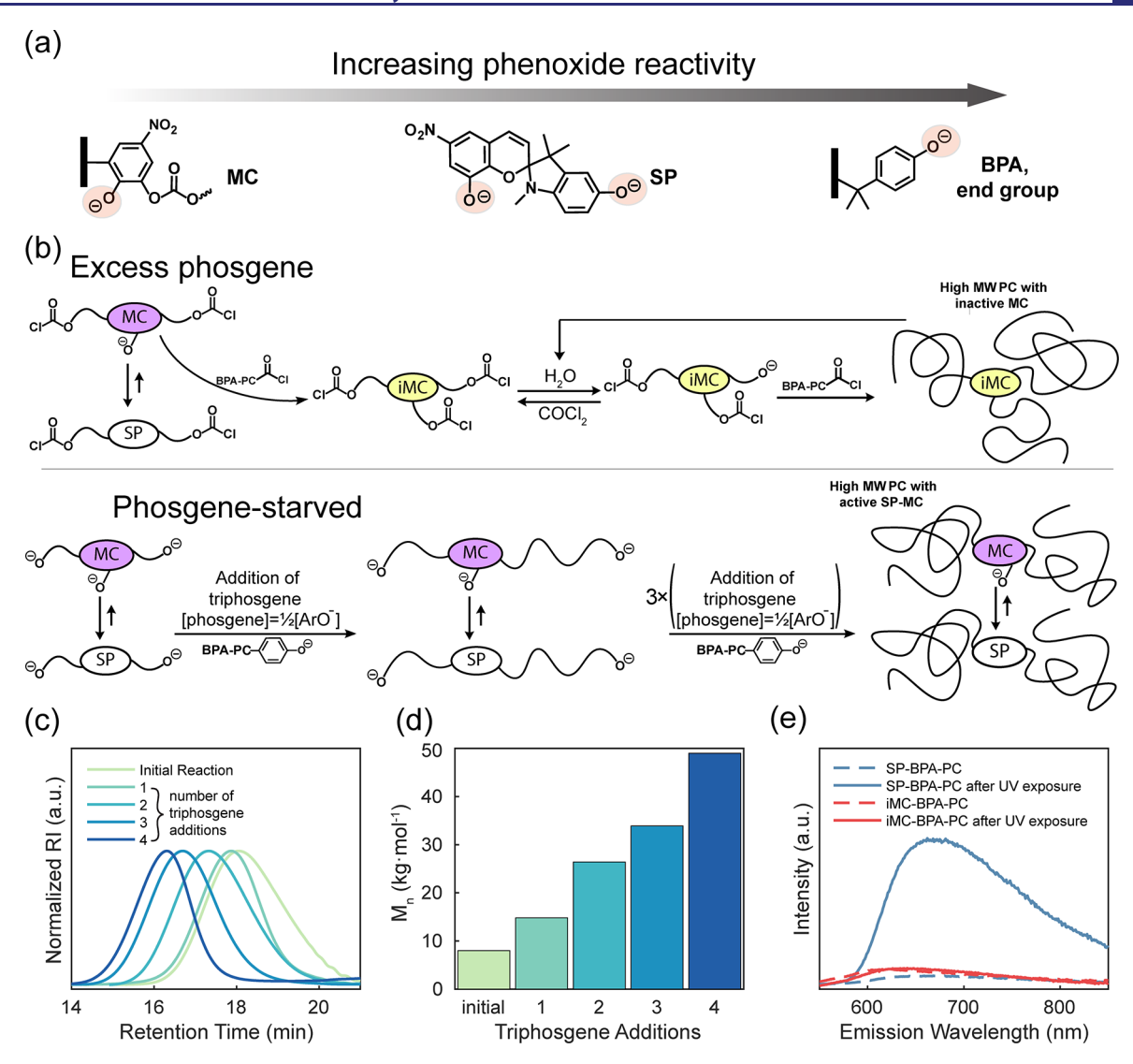


Figure 3. (a) Relative reactivities of MC, SP, and BPA-derived phenoxides toward phosgene or chloroformate end-groups. (b) Formation of the inactive iMC species during SP-BPA-PC synthesis in the presence of excess phosgene and retention of the active SP-MC species by using phosgene-starved conditions. (c) GPC plots show the lower retention time (higher  $M_n$ ) after each addition of triphosgene. (d)  $M_n$  after each addition of triphosgene. (e) 532 nm excitation fluorescence spectra in  $CH_2Cl_2$  of active SP-BPA-PC synthesized under phosgene starved conditions (blue) and iMC-BPA-PC synthesized under excess phosgene conditions (red) before and after exposure to 365 nm light.

the synthesized SP-BPA-PC in dichloromethane exhibited the desired reversible photochromism when alternatively irradiated with UV and white light (Figure S4). In the solid state, the SP-BPA-PC does not photoisomerize, while the nonbonded SP dispersed in commercial PC can reversibly isomerize upon irradiation, verifying the covalent attachment of SP in the SP-BPA-PC backbone (Figure S10). To corroborate the assumption that phosgene excess causes the loss of SP-MC activity, the active SP-BPA-PC was exposed to triphosgene ([phosgene] > [phenol]) under basic conditions, presumably forming iMC-BPA-PC. The fluorescence emission spectra after exposure to UV light for SP-BPA-PC show the MC typical broad peak around 690 nm that is not observed before or after UV exposure of the iMC-BPA-PC (Figure 3e).

**Mechanical Characterization.** Simultaneous Measurement of Stress, Strain, and Fluorescence. Characterization of mechanically driven spiropyran to merocyanine conversion was obtained by simultaneous tensile testing and fluorescence imaging (Figure 4a). Fluorescence was excited by a 532 nm

laser source and imaged through a long-pass filter to detect the fluorescence peak of MC<sup>26</sup> (Figure S11). Between images, a mechanical shutter blocks the laser source to minimize photobleaching. Relative changes in the activation of spiropyran are quantified by measuring the fluorescence intensity in the center region of the tensile specimen (Figure 4b). Even though SP-BPA-PC is a stiff glassy polymer with an elastic modulus of ~1.9 GPa, it is also highly stretchable with a maximum elongation of over 100%. Like conventional polycarbonate, the mechanical response of SP-BPA-PC starts with linear elasticity followed by a distinct yield peak, softening, and strain hardening. From the change in fluorescence intensity, we observed that activation of SP occurs after yield and continues to increase while the material strain hardens (Figure 4c). When viewed under white light, the specimen stretched past it's yield point exhibits a vibrant purple color (movie S1). Upon force removal, activated SP maintains its color (Figure 4d). It has been shown in the literature that attachment on both sides of the SP molecule is

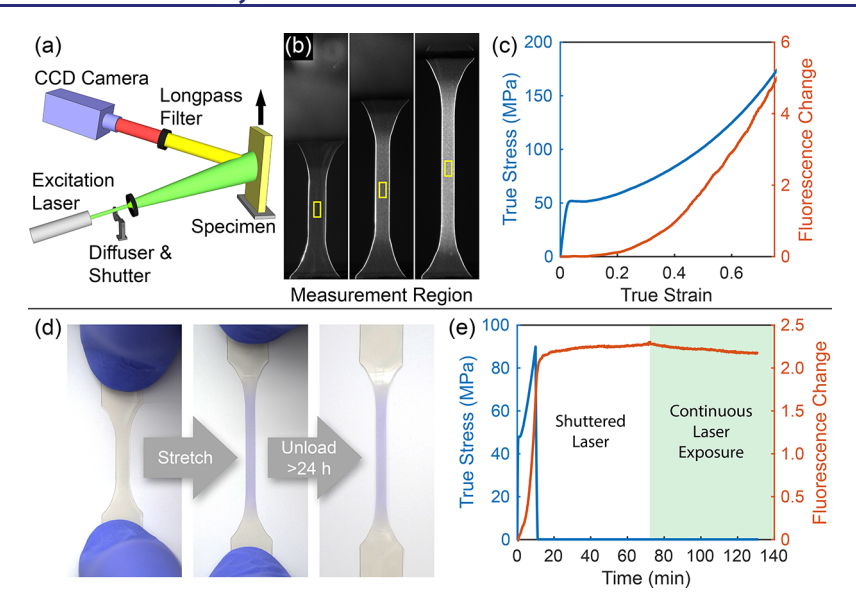
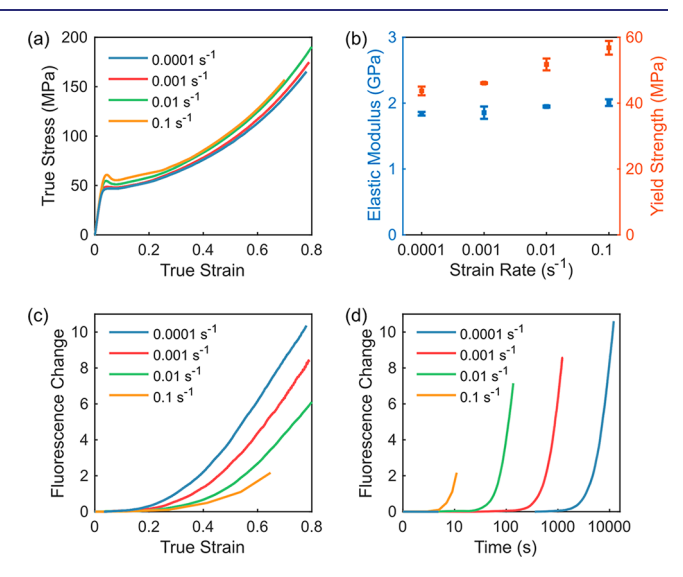


Figure 4. (a) Schematic of the experimental system for concurrent fluorescence measurement and uniaxial tensile deformation of SP-BPA-PC specimen. (b) Fluorescence images of SP-BPA-PC subjected to uniaxial tensile deformation with the fluorescence intensity measurement region denoted by the yellow rectangle. (c) True stress versus strain versus fluorescence change for a typical monotonic tensile test. (d) Purple color of a stretched specimen when viewed under visible light. The purple color is maintained after 24 h. (e) Stress and fluorescence change over time when a specimen is stretched to 0.47 true strain and unloaded.

essential for force transmission across the C<sub>spiro</sub>-O bond, allowing efficient mechanochemical activation. <sup>15,16,46</sup> To rule out other mechanisms such as local heating and molecular friction, <sup>47</sup> we compared the SP-BPA-PC with SP dispersed in BPA-PC. The unattached SP molecules, which can photoisomerize, do not produce a significant change in fluorescence upon tensile loading (Figure S12), supporting the mechanism of force driven activation in SP-BPA-PC.

In a separate experiment, the SP activation of a specimen loaded past yield was monitored after unloading for 1 h with the laser shuttered between images and for another hour with continuous light exposure. Under dark conditions with the laser shutter, SP activation continues slowly after stress release with fluorescence increasing by 15% over 1 h. When the specimen is continuously exposed to the laser, there is a slight decrease (6%) in fluorescence after 1 h. The persistent mechanochromic response after stress release is ideal for indicating the associated prior deformation.

Monotonic Loading. To evaluate SP activation under varying mechanical histories, we stretched SP-BPA-PC at strain rates spanning four decades. Figure 5a shows that the stressstrain response is comparable when loaded at varying rates with slightly higher stress at faster rates. Under closer examination, Figure 5b shows that the initial elastic behavior is insensitive to strain rate with moduli between 1.8 and 2 GPa. The yield strengths for the slower rates of 0.0001 and 0.001 s<sup>-1</sup> are similar, averaging at 44 and 46 MPa, respectively, whereas the faster rates of 0.01 and 0.1 s<sup>-1</sup> result in higher yield strengths of 52 and 57 MPa, respectively. Despite similar stresses, SP activation depends strongly on the strain rate. Figure 5c shows that fluorescence at a given strain is higher for slower strain rates. While this may seem contradictory at first glance because higher strain rates result in higher stresses and presumably higher forces to drive mechanophore activation, the slower strain rates provide more time for SP to MC conversion and molecular mechanisms that enable this conversion. 13,30 A finite amount of time is required for the



**Figure 5.** Strain rate effect during monotonic uniaxial loading. (a) Stress—strain response, (b) elastic modulus and yield stress versus strain rate, (c) fluorescence change versus strain, and (d) fluorescence change versus time.

polymer chains to reach a configuration in which force is applied across the SP (e.g., when chains are aligned with the loading direction). S,47,48 The polymer chain reorientation time scale ( $\tau$ ), which can be inferred from the initial rates of stress relaxation, 49,50 ranges from 30 to 70 s during plastic flow (Figure S13). The test time for the fastest strain rate experiment is shorter than the relaxation time scale ( $t_{\text{test}} \approx 0.3-0.7\tau$ ) while the slowest strain rate experiments are longer ( $t_{\text{test}} \approx 2-400\tau$ ), allowing more time for chain reorientation. The effect of time for the mechanochemical reaction to occur is made clear from the differences in fluorescence for the 0.0001 and 0.001 s<sup>-1</sup> experiments, which have nearly identical stresses. When fluorescence is compared against time (Figure 5d), it is clear that SP to MC conversion happens faster at

higher strain rates. The approximate order of magnitude difference in SP activation rates corresponds to the order of magnitude differences in strain rates among the tests.

Cyclic and Stress Relaxation Loading. Because SP activation has complex interactions with stress, deformation, and time, we devised experiments that alter one parameter while controlling the others. In the previously described monotonic tensile tests, the amount of stress primarily depended on strain. With different strain rates, we can observe SP activation under different test times, while keeping stress and strain comparable between tests. To study SP activation with varying stresses, we performed cyclic and stress relaxation tests, which result in different stress histories while controlling strain and test time. For cyclic tests, we stretched the specimen to increments of 0.1 engineering strain and, at each increase, cycled down to zero load three times. During these cycles, the stress decreased ca. 5% upon each reload. In addition to the expected increase in fluorescence while stretching, there is also a smaller overall increase in fluorescence during the cycles with larger changes at higher strain increments (Figure 6a). For the

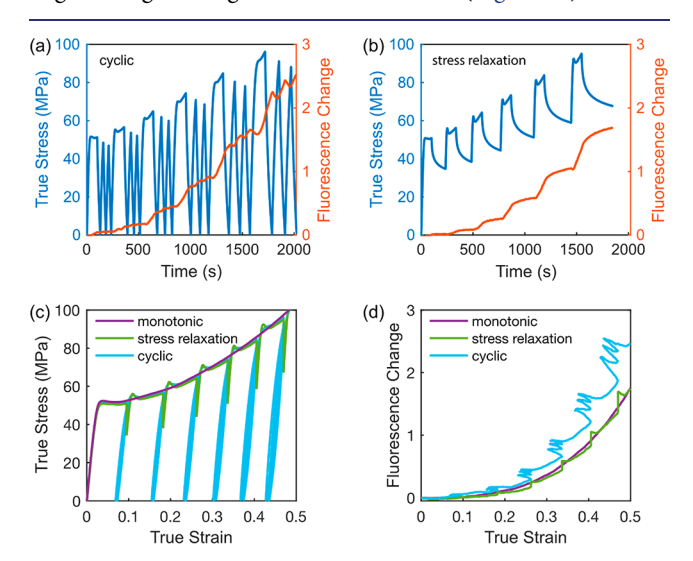


**Figure 6.** Comparison of stress and fluorescence for monotonic, cyclic, and stress relaxation loading. Stress versus time versus fluorescence change for (a) cyclic test and (b) stress relaxation test. (c) Stress versus strain and (d) fluorescence change versus strain for monotonic, stress relaxation, and cyclic tests.

stress relaxation test, we stretched the specimen to increments of 0.1 strain and held at constant strain for the same duration as the corresponding cyclic test cycles. When holding the specimen at constant strain, the stress decreases rapidly and then approaches a plateau. During this time, the fluorescence increases, albeit at a slower rate than during loading (Figure 6b).

The stress—strain responses of the three loading histories (Figure 6c) are overall similar the first time a strain is reached. During the hold time for the stress—relaxation tests, the stress drops; when the strain is increased again, there is a slight overshoot before the stress drops back down to the monotonic stress. Similarly, the cyclic stress response slightly overshoots the monotonic stress upon reloading. Critically, the average stress for the stress relaxation and cyclic tests is 9% and 40% lower than the monotonic tests, respectively, when averaged over the duration of each experiment. The cyclic and stress relaxation tests take nearly the same amount of time as each

other and ~3 times longer than the monotonic test. Comparing the stress relaxation and monotonic fluorescence, it appears that, despite the lower average stress, the fluorescence for the stress relaxation sequence is slightly higher than the monotonic loading (Figure 6d). However, this comparison is convoluted because the stress relaxation specimen is exposed to stress over longer times. It appears that, while stress hold times can mildly increase fluorescence, this does not strongly stimulate the mechanochemical reaction. Under cyclic loading, the increase in fluorescence at each strain is significantly higher as compared to the monotonic and stress relaxation sequences. For instance, at a true strain of 0.47, the cyclic test has a fluorescence value of 2.5, whereas the stress relaxation test has a fluorescence of 1.7 and the monotonic test has a fluorescence of 1.4. The comparison between cyclic and stress relaxation is direct because the total test time is matched. This shows that average stress over time does not predict mechanochemical activation. Because it is well-known that cyclic loading can cause PC to fail at reduced strains as compared to monotonic loading, 51 we consider this increase in fluorescence with cyclic loading to be a desirable feature. The contrast among fluorescence behavior under monotonic, stress relaxation, and cyclic loading is reminiscent of the glassy polymer micromechanics plasticity literature. Inelasticity occurs through shear transformation zones that develop inhomogeneously throughout the material, opening up free volume to enable molecular mobility. This evolution varies with both loading rate and loading history. 52-58 Stress relaxation loading provides more time than the monotonic loading at each strain for the microstructure to evolve, whereas the cyclic loading directly stimulates this evolution.

Mechanosensing in a SP-BPA-PC Laminate. To validate the potential for SP-BPA-PC as a sensor that reveals mechanical history, we implemented it as a film that can be laminated onto a bulk plastic. The film provides a 2D fluorescence field that indicates plasticity with high spatial resolution. Because the laminate can be used to place mechanophores in relevant locations (e.g., visible surfaces), this approach reduces the quantity of costly mechanophores when compared to uniformly distributed mechanophores in bulk structures. To support our proof of concept, the SP-BPA-PC fluorescence field was compared to digital image correlation (DIC), a widely adopted method for full-field deformation measurement. Yet, SP-BPA-PC sensors have unique advantages over DIC: (i) In contrast to DIC, which requires continuous monitoring to ensure image correlation, SP-BPA-PC film can be left unattended and provides information via persistent SP activation. (ii) SP-BPA-PC indicates plasticity, which predicates material failure, whereas DIC reports strain and displacement. (iii) The resulting fluorescence field is observable by visual inspection with a UV light, whereas DIC measurements require image processing software. Together, these features make SP-BPA-PC ideal for use as plastic deformation warning indicators.

The SP-BPA-PC film was incorporated onto a polycarbonate beam with a light-cure adhesive and tested using four-point bending (Figure 7). The resulting red fluorescence field (Figure 7b) was then compared to strain measurements obtained by DIC on an identical beam with the same loading (Figure 7c). We bent the beams in increments of 2 mm displacement and captured the fluorescence and DIC field at each increment. Four-point bending generates longitudinal  $(\varepsilon_{xx})$  strain between the two indenters that has its maximum

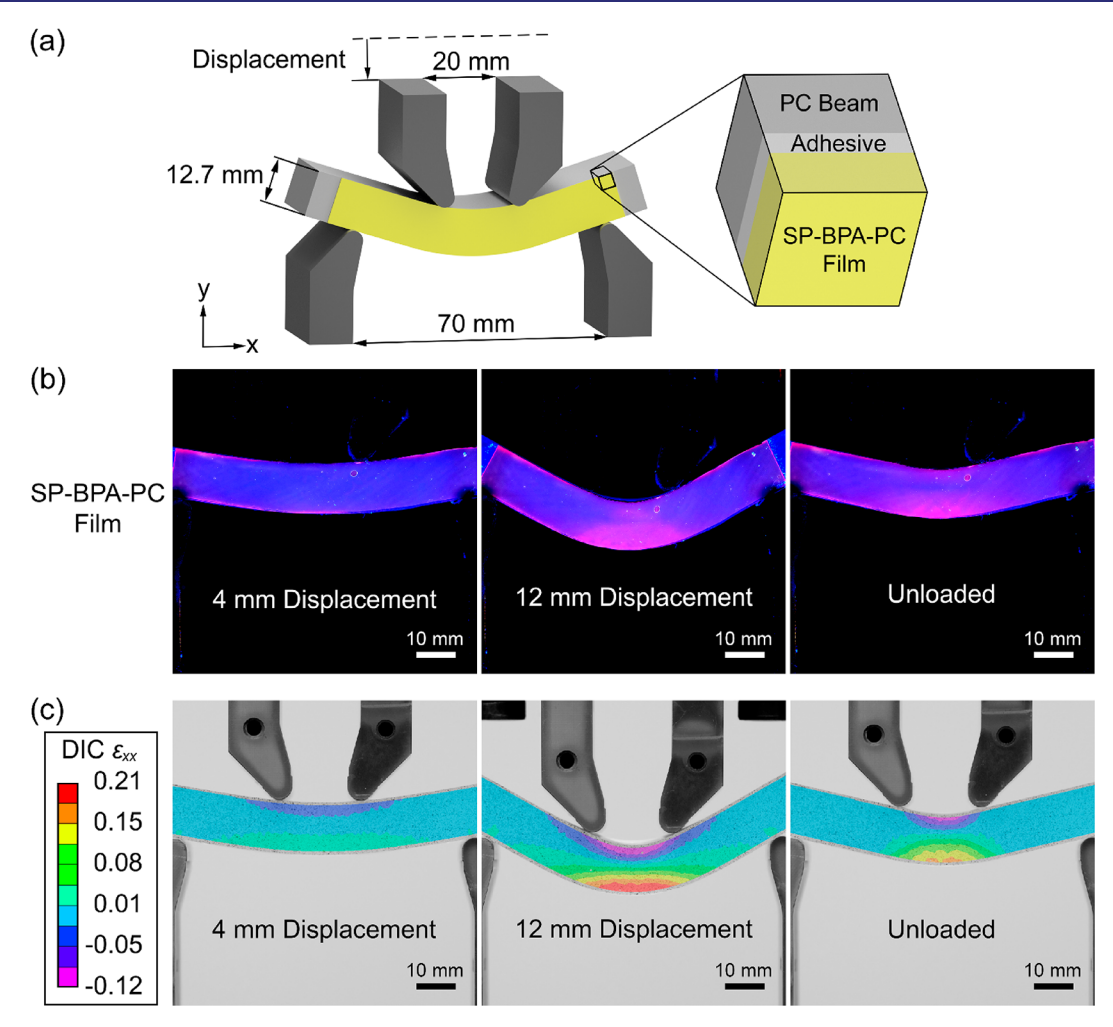


Figure 7. (a) Schematic of SP-BPA-PC film laminated onto a polycarbonate beam subjected to four-point bending. (b) SP fluorescence field and (c) digital image correlation axial strain  $(\varepsilon_{xx})$  measurement during beam bending at 4 mm displacement, 12 mm displacement, and after unloading to zero force.

tensile values at the bottom surface and increases to the maximum compressive value at the upper surface. At small deformations, the  $\varepsilon_{xx}$  compressive and tensile strains are mirrored around the center; however, at large displacements, the strain on the faces are nonsymmetric. Four-point bending to large displacement also results in transverse  $(\varepsilon_{yy})$  strain and shear  $(\varepsilon_{xy})$  strain. In the bottom-center of the beam, we see compressive  $\varepsilon_{yy}$  strains that are up to 60% of the  $\varepsilon_{xx}$  strain, while everywhere else,  $\varepsilon_{vv}$  and  $\varepsilon_{xv}$  are considerably lower than the  $\varepsilon_{xx}$  strains (Figure S14 and movie S2).

When the beam was bent elastically (to 4 mm deflection), the SP-BPA-PC film did not show activation. We measured the red channel intensity of the image for a  $5 \times 5$  mm region on the top and bottom edges of the center of the beam. Initially, the signal was 152 for the top and 138 for the bottom, which after 4 mm deflection changed to 152 and 141, respectively. The DIC analysis showed a strain field with average  $\varepsilon_{xx}$  strain on the top of -0.02 and on the bottom of 0.02. When the beam was bent plastically to 12 mm deflection, the SP-BPA-PC film showed activation at the bottom region, with the red channel intensity increasing to 196. This coincides with average  $\varepsilon_{xx}$  strains of 0.17. In the upper part of the beam,  $\varepsilon_{xx}$ strains average at -0.04, which results in faint fluorescence with a red channel value of 166, indicating little activation. SP activation under compression of a glassy polymer was

demonstrated in prior work,<sup>30</sup> so we expect that this small degree of activation is primarily due to the small strain value rather than a tension versus compression difference. Upon unloading, SP-BPA-PC fluorescence in the plastically deformed regions remained with a red value of 198 in the bottom region and 152 in the top region, whereas the DIC measurement shows a reduction in strain with average  $\varepsilon_{xx}$  of 0.12 for the bottom and -0.03 for the top due to elastic recovery. Although the total beam deflection of the unloaded beam is similar to loading to 4 mm, the mechanical history of the beam is evident from the difference in fluorescence field with peak fluorescence equal to that at max loading.

#### CONCLUSIONS

We have introduced the mechanoactive spiropyran functionality into a polycarbonate backbone while retaining its excellent thermomechanical properties. We avoided the typical low yield SP functionalization step, by utilizing the bisphenol structure of dihydroxyspiropyran directly in the polycondensation reaction. Spiropyran-polycarbonate is the first glassy polymer that has been shown to exhibit room-temperature mechanochromic activation under tensile loading without any additives. This model system allows us to understand how the complex interactions between stress, deformation, and time contribute to spiropyran activation in glassy polymers. Spiropyran activation correlates with strain after yield, but rate and strain history are also key factors. Cyclic loading stimulates considerably higher activation as compared to monotonic loading, suggesting chain rearrangement during the unloading cycles. In addition, the higher activation under cyclic loading demonstrates the desirable enhanced activation in response to loading that promotes failure. Moreover, the persistent activation of SP after force removal enables on demand inspection rather than requiring continuous tracking (a requirement for DIC). Laminates were shown to be an effective way for adding mechanochromic functionality to structures and follow surface deformation while reducing the use of costly mechanophores. We laminated SP-BPA-PC film onto conventional polycarbonate to visualize surface deformation with a 2D fluorescence field under four-point bending. The laminate fluorescence reflected the maximum loading case experienced by the beam. These developments of efficient processes for employing mechanophores and room-temperature activation in stiff materials bring us closer to using mechanochromic materials as damage sensors in high performance engineered plastics.

## ASSOCIATED CONTENT

## **S** Supporting Information

The Supporting Information is available free of charge on the ACS Publications website at DOI: 10.1021/jacs.9b04229.

Synthetic procedures, chemical and mechanical characterization data, material processing, and film lamination procedure (PDF)

# AUTHOR INFORMATION

## **Corresponding Author**

\*ms2682@cornell.edu

#### **ORCID** ®

Yuval Vidavsky: 0000-0003-1727-7607 Brooks A. Abel: 0000-0002-2288-1975 Geoffrey W. Coates: 0000-0002-3400-2552 Meredith N. Silberstein: 0000-0002-6853-9796

# **Author Contributions**

"Y.V. and S.J.Y. contributed equally to this work.

#### Notes

The authors declare no competing financial interest.

#### ACKNOWLEDGMENTS

This research was funded by the National Science Foundation under Grant no. CMMI-1653059 and by the Israel Science Foundation (grant 920/15). This research made use of the NMR Facility at Cornell University that was supported in part by the NSF under award CHE-1531632, and the Cornell Center for Materials Research Shared Facilities, which are supported through the NSF MRSEC program (DMR-1719875).

## REFERENCES

- (1) Simon, Y. C.; Craig, S. L. Mechanochemistry in Materials; Royal Society of Chemistry: UK, 2017; Vol. 26.
- (2) May, P. A.; Moore, J. S. Polymer Mechanochemistry: Techniques to Generate Molecular Force via Elongational Flows. *Chem. Soc. Rev.* **2013**, 42, 7497–7506.
- (3) Black, A. L.; Lenhardt, J. M.; Craig, S. L. From Molecular Mechanochemistry to Stress-Responsive Materials. *J. Mater. Chem.* **2011**, *21*, 1655–1663.

- (4) Li, J.; Nagamani, C.; Moore, J. S. Polymer Mechanochemistry: From Destructive to Productive. *Acc. Chem. Res.* **2015**, *48*, 2181–2190.
- (5) Diesendruck, C. E.; Steinberg, B. D.; Sugai, N.; Silberstein, M. N.; Sottos, N. R.; White, S. R.; Braun, P. V.; Moore, J. S. Proton-Coupled Mechanochemical Transduction: A Mechanogenerated Acid. *J. Am. Chem. Soc.* **2012**, *134*, 12446–12449.
- (6) Piermattei, A.; Karthikeyan, S.; Sijbesma, R. P. Activating Catalysts with Mechanical Force. *Nat. Chem.* **2009**, *1*, 133–137.
- (7) Robb, M. J.; Li, W.; Gergely, R. C. R.; Matthews, C. C.; White, S. R.; Sottos, N. R.; Moore, J. S. A Robust Damage-Reporting Strategy for Polymeric Materials Enabled by Aggregation-Induced Emission. *ACS Cent. Sci.* **2016**, *2*, 598–603.
- (8) Raisch, M.; Genovese, D.; Zaccheroni, N.; Schmidt, S. B.; Focarete, M. L.; Sommer, M.; Gualandi, C. Highly Sensitive, Anisotropic, and Reversible Stress/Strain-Sensors from Mechanochromic Nanofiber Composites. *Adv. Mater.* **2018**, *30*, 1802813.
- (9) Ducrot, E.; Chen, Y.; Bulters, M.; Sijbesma, R. P.; Creton, C. Toughening Elastomers with Sacrificial Bonds and Watching Them Break. *Science* **2014**, 344, 186–189.
- (10) Hu, X.; McFadden, M. E.; Barber, R. W.; Robb, M. J. Mechanochemical Regulation of a Photochemical Reaction. *J. Am. Chem. Soc.* **2018**, *140*, 14073–14077.
- (11) Chen, Y.; Spiering, A. J. H.; Karthikeyan, S.; Peters, G. W. M.; Meijer, E. W.; Sijbesma, R. P. Mechanically Induced Chemiluminescence from Polymers Incorporating a 1,2-Dioxetane Unit in the Main Chain. *Nat. Chem.* **2012**, *4*, 559–562.
- (12) Gossweiler, G. R.; Kouznetsova, T. B.; Craig, S. L. Force-Rate Characterization of Two Spiropyran-Based Molecular Force Probes. *J. Am. Chem. Soc.* **2015**, *137*, 6148–6151.
- (13) Kim, T. A.; Beiermann, B. A.; White, S. R.; Sottos, N. R. Effect of Mechanical Stress on Spiropyran-Merocyanine Reaction Kinetics in a Thermoplastic Polymer. *ACS Macro Lett.* **2016**, *5*, 1312–1316.
- (14) Beiermann, B. A.; Kramer, S. L. B.; May, P. A.; Moore, J. S.; White, S. R.; Sottos, N. R. The Effect of Polymer Chain Alignment and Relaxation on Force-Induced Chemical Reactions in an Elastomer. *Adv. Funct. Mater.* **2014**, 24, 1529–1537.
- (15) Li, M.; Zhang, Q.; Zhou, Y. N.; Zhu, S. Let Spiropyran Help Polymers Feel Force! *Prog. Polym. Sci.* **2018**, *79*, 26–39.
- (16) Davis, D. A.; Hamilton, A.; Yang, J.; Cremar, L. D.; Van Gough, D.; Potisek, S. L.; Ong, M. T.; Braun, P. V.; Martinez, T. J.; White, S. R.; Moore, J. S.; Sottos, N. R. Force-Induced Activation of Covalent Bonds in Mechanoresponsive Polymeric Materials. *Nature* **2009**, 459, 68–72.
- (17) Lin, Y.; Barbee, M. H.; Chang, C.; Craig, S. L. Regiochemical Effects on Mechanophore Activation in Bulk Materials. *J. Am. Chem. Soc.* **2018**, *140*, 15969–15975.
- (18) Chen, Y.; Zhang, H.; Fang, X.; Lin, Y.; Xu, Y.; Weng, W. Mechanical Activation of Mechanophore Enhanced by Strong Hydrogen Bonding Interactions. ACS Macro Lett. 2014, 3, 141–145.
- (19) Wang, Q.; Gossweiler, G. R.; Craig, S. L.; Zhao, X. Cephalopod-Inspired Design of Electro-Mechano-Chemically Responsive Elastomers for on-Demand Fluorescent Patterning. *Nat. Commun.* **2014**, *5*, 4899.
- (20) O'Bryan, G.; Wong, B. M.; McElhanon, J. R. Stress Sensing in Polycaprolactone Films via an Embedded Photochromic Compound. ACS Appl. Mater. Interfaces 2010, 2, 1594–1600.
- (21) Jiang, S.; Zhang, L.; Xie, T.; Lin, Y.; Zhang, H.; Xu, Y.; Weng, W.; Dai, L. Mechanoresponsive PS-PnBA-PS Triblock Copolymers via Covalently Embedding Mechanophore. *ACS Macro Lett.* **2013**, *2*, 705–709.
- (22) Lee, C. K.; Diesendruck, C. E.; Lu, E.; Pickett, A. N.; May, P. A.; Moore, J. S.; Braun, P. V. Solvent Swelling Activation of a Mechanophore in a Polymer Network. *Macromolecules* **2014**, *47*, 2690–2694.
- (23) Li, M.; Liu, W.; Zhu, S. Smart Polyolefins Feeling the Force: Color Changeable Poly(Ethylene-Vinyl Acetate) and Poly(Ethylene-Octene) in Response to Mechanical Force. *Polymer* **2017**, *112*, 219–227.

- (24) Gossweiler, G. R.; Hewage, G. B.; Soriano, G.; Wang, Q.; Welshofer, G. W.; Zhao, X.; Craig, S. L. Mechanochemical Activation of Covalent Bonds in Polymers with Full and Repeatable Macroscopic Shape Recovery. *ACS Macro Lett.* **2014**, *3*, 216–219.
- (25) Lee, C. K.; Beiermann, B. A.; Silberstein, M. N.; Wang, J.; Moore, J. S.; Sottos, N. R.; Braun, P. V. Exploiting Force Sensitive Spiropyrans as Molecular Level Probes. *Macromolecules* **2013**, *46*, 3746–3752.
- (26) Beiermann, B. A.; Kramer, S. L. B.; Moore, J. S.; White, S. R.; Sottos, N. R. Role of Mechanophore Orientation in Mechanochemical Reactions. *ACS Macro Lett.* **2012**, *1*, 163–166.
- (27) Grady, M. E.; Beiermann, B. A.; Moore, J. S.; Sottos, N. R. Shockwave Loading of Mechanochemically Active Polymer Coatings. *ACS Appl. Mater. Interfaces* **2014**, *6*, 5350–5355.
- (28) Beiermann, B. A.; Davis, D. A.; Kramer, S. L. B.; Moore, J. S.; Sottos, N. R.; White, S. R. Environmental Effects on Mechanochemical Activation of Spiropyran in Linear PMMA. *J. Mater. Chem.* **2011**, 21, 8443–8447.
- (29) Kingsbury, C. M.; May, P. A.; Davis, D. A.; White, S. R.; Moore, J. S.; Sottos, N. R. Shear Activation of Mechanophore-Crosslinked Polymers. *J. Mater. Chem.* **2011**, 21, 8381–8388.
- (30) Kim, J. W.; Jung, Y.; Coates, G. W.; Silberstein, M. N. Mechanoactivation of Spiropyran Covalently Linked PMMA: Effect of Temperature, Strain Rate, and Deformation Mode. *Macromolecules* **2015**. *48*. 1335–1342.
- (31) Silberstein, M. N.; Min, K.; Cremar, L. D.; Degen, C. M.; Martinez, T. J.; Aluru, N. R.; White, S. R.; Sottos, N. R. Modeling Mechanophore Activation within a Crosslinked Glassy Matrix. *J. Appl. Phys.* **2013**, *114*, 23504.
- (32) Silberstein, M. N.; Cremar, L. D.; Beiermann, B. A.; Kramer, S. B.; Martinez, T. J.; White, S. R.; Sottos, N. R. Modeling Mechanophore Activation within a Viscous Rubbery Network. *J. Mech. Phys. Solids* **2014**, *63*, 141–153.
- (33) Potisek, S. L.; Davis, D. A.; Sottos, N. R.; White, S. R.; Moore, J. S. Mechanophore-Linked Addition Polymers. *J. Am. Chem. Soc.* **2007**, *129*, 13808–13809.
- (34) Lee, C. K.; Davis, D. A.; White, S. R.; Moore, J. S.; Sottos, N. R.; Braun, P. V. Force-Induced Redistribution of a Chemical Equilibrium. *J. Am. Chem. Soc.* **2010**, *132*, 16107–16111.
- (35) Peterson, G. I.; Larsen, M. B.; Ganter, M. A.; Storti, D. W.; Boydston, A. J. 3D-Printed Mechanochromic Materials. *ACS Appl. Mater. Interfaces* **2015**, *7*, 577–583.
- (36) Li, M.; Liu, W.; Zhang, Q.; Zhu, S. Mechanical Force Sensitive Acrylic Latex Coating. ACS Appl. Mater. Interfaces 2017, 9, 15156—15163.
- (37) Bendler, J.; LeGrand, D. Handbook of Polycarbonate Science and Technology; Marcel Dekker Inc.: New York, 2000.
- (38) Caswell, S. V.; Gould, T. E.; Wiggins, J. S. *Materials in Sports Equipment*; Woodhead Publishing: Cambridge, England, 2007; Vol. 2, pp 87–126.
- (39) Clayton, K.; Milholland, J.; Stenger, G. Experimental Evaluation of F-16 Polycarbonate Canopy Material, 1981; p 129.
- (40) Shah, Q. H. Impact Resistance of a Rectangular Polycarbonate Armor Plate Subjected to Single and Multiple Impacts. *Int. J. Impact Eng.* **2009**, *36*, 1128–1135.
- (41) Cotarca, L.; Geller, T.; Répási, J. Bis(Trichloromethyl)-Carbonate (BTC, Triphosgene): A Safer Alternative to Phosgene? Org. Process Res. Dev. 2017, 21, 1439–1446.
- (42) Eckert, H.; Forster, B. Triphosgene, a Crystalline Phosgene Substitute. *Angew. Chem., Int. Ed. Engl.* **1987**, *26*, 894–895.
- (43) Minkin, V. I. Photo-, Thermo-, Solvato-, and Electrochromic Spiroheterocyclic Compounds. *Chem. Rev.* **2004**, *104*, 2751–2776.
- (44) Calculated Using Advanced Chemistry Development (ACD/Labs) Software V11.02 (1994–2019 ACD/Labs).
- (45) Um, S.; Kwon, Y.; Han, H.; Park, S.; Park, M.; Rho, Y.; Sin, H. Synthesis and Biological Activity of Novel Retinamide and Retinoate Derivatives. *Chem. Pharm. Bull.* **2004**, *52*, 501–506.

- (46) Qiu, W.; Gurr, P. A.; da Silva, G.; Qiao, G. G. Insights into the Mechanochromism of Spiropyran Elastomers. *Polym. Chem.* **2019**, *10*, 1650–1659.
- (47) Beiermann, B. A.; Kramer, S. L. B.; May, P. A.; Moore, J. S.; White, S. R.; Sottos, N. R. The Effect of Polymer Chain Alignment and Relaxation on Force-Induced Chemical Reactions in an Elastomer. *Adv. Funct. Mater.* **2014**, 24, 1529–1537.
- (48) Degen, C. M.; May, P. A.; Moore, J. S.; White, S. R.; Sottos, N. R. Time-Dependent Mechanochemical Response of SP-Cross-Linked PMMA. *Macromolecules* **2013**, *46*, 8917–8921.
- (49) Bending, B.; Ediger, M. D. Comparison of Mechanical and Molecular Measures of Mobility during Constant Strain Rate Deformation of a PMMA Glass. *J. Polym. Sci., Part B: Polym. Phys.* **2016**, *54*, 1957–1967.
- (50) Kim, J. W.; Medvedev, G. A.; Caruthers, J. M. Nonlinear Stress Relaxation in an Epoxy Glass and Its Relationship to Deformation Induced Mobility. *Polymer* **2013**, *54*, 3949–3960.
- (51) Rabinowitz, S.; Beardmore, P. Cyclic Deformation and Fracture of Polymers. *J. Mater. Sci.* **1974**, *9*, 81–99.
- (52) Stachurski, Z. H. Deformation Mechanisms and Yield Strength in Amorphous Polymers. *Prog. Polym. Sci.* **1997**, 22, 407–474.
- (53) Shenogin, S.; Ozisik, R. Deformation of Glassy Polycarbonate and Polystyrene: The Influence of Chemical Structure and Local Environment. *Polymer* **2005**, *46*, 4397–4404.
- (54) Argon, A. S.; Bessonov, M. I. Plastic Flow in Glassy Polymers. *Polym. Eng. Sci.* **1977**, *17*, 174–182.
- (55) Hasan, O. A.; Boyce, M. C.; Li, X. S.; Berko, S. An Investigation of the Yield and Postyield Behavior and Corresponding Structure of Poly(Methyl Methacrylate). *J. Polym. Sci., Part B: Polym. Phys.* **1993**, 31, 185–197.
- (56) Hasan, O. A.; Boyce, M. C. Energy Storage during Inelastic Deformation of Glassy Polymers. *Polymer* **1993**, *34*, 5085–5092.
- (57) Oleinik, E. F.; Mazo, M. A.; Strel'nikov, I. A.; Rudnev, S. N.; Salamatina, O. B. Plasticity Mechanism for Glassy Polymers: Computer Simulation Picture. *Polym. Sci., Ser. A* **2018**, *60*, 1–49.
- (58) Capaldi, F. M.; Boyce, M. C.; Rutledge, G. C. Molecular Response of a Glassy Polymer to Active Deformation. *Polymer* **2004**, 45, 1391–1399.